Soft Matter

PAPER

View Article Online
View Journal | View Issue

Cite this: *Soft Matter*, 2020, **16**, 8710

Cluster prevalence in concentrated ring-chain mixtures under shear

Maximilian Liebetreu * and Christos N. Likos

Semiflexible ring polymers are known to exhibit clustering behavior and form stacks in concentrated solutions. Recently, weak shear was suggested to re-orient these stacks with flow, a phenomenon more easily visible in more concentrated solutions [Liebetreu *et al.*, *ACS Appl. Polym. Mater.*, 2020, **2**(8), 3505–3517, DOI: 10.1021/acsapm.0c00522]. In this work, we investigate the impact of mixing linear chains and rings in a similar system under shear, studying clustering in the presence of semiflexible, rod-like chains. We present a correlation between chain monomer fraction and clustering behavior as linear chains take up less space, thus decreasing the system's effective density and, subsequently, clustering. However, we suggest mixtures with a low chain concentration to maintain or potentially enhance clustering at equilibrium while this effect is destroyed under shear. The mixing of chains and rings may therefore be used to create more strongly organized structures susceptible to reorientation *via* weak shear.

Received 17th July 2020,
Accepted 28th August 2020

DOI: 10.1039/d0sm01309a

rsc.li/soft-matter-journal

1 Introduction

In recent years, the importance of polymer topology for dynamical and rheological properties has gained significant importance. Polymers come in a host of different topologies such as linear chains, stars, dendrimers and rings, and the impact of topological differences on polymer dynamics in dilute solution has been studied extensively both in equilibrium[1–5] and a variety of out-of-equilibrium situations[6–8] such as shear flow. Special attention has been given to dynamics under spatial constraints,[9–11] and it has recently been shown that linear chains and rings move through narrow segmented channels at different radial distances.[12] Spatial constraints imposed *via* an increase of monomer density have also been studied extensively for melts[13,14] as well as semi-dilute suspensions.[15,16]

Polymers of diverse topology often occur naturally. Examples for ring-shaped polymers include plasmids and the kinetoplast from the mitochondria of trypanosome parasites.[17] Synthetically, polymer topology can be controlled through the use of optical tweezers,[18] and double-stranded DNA rings have been manufactured to produce catenanes,[19–23] a group of interlinked rings.

Semiflexible rings in concentrated solutions are known to exhibit a self-organized, amorphous cluster phase in equilibrium.[15,16,24] In this phase, rings form long stacks without net translational and orientational order. On such stacks, rings are strongly correlated to each other as well as to rings on neighboring stacks. These rings are typically of oblate shape, but some of them may also exhibit a prolate shape and thread through other rings in order to reside within a given stack. Dynamically, the cluster phase results in a cluster glass,[25] an arrested form of matter in which the cluster structures are locked into place but individual rings can hop between clusters, similar to individual particles in cluster crystals.[26] In addition to pure ring solutions or melts, mixtures of rings and linear chains have also attracted considerable attention recently, both theoretically and experimentally, due to the rich dynamics they display, and in particular with a focus on the mechanism of threading of the rings by the chain and the ensuing constraint release mechanism.[27–33] Furthermore, mixtures of long linear chains and polymer rings have been shown to exhibit an increased viscosity as compared to pure chain solutions.[34–36]

Recently, semiflexible rings have been shown to exhibit pronounced clustering behavior even under weak shear, whereas strong shear destroys clusters.[37] Such sheared clusters have been shown to re-orient due to the imposed shear and form bands aligned with flow independent of consideration or disregard of fully-developed hydrodynamic interactions. Stacks aligned in this manner maintain their orientation even after cessation of shear. This effect is more pronounced in concentrated solutions and more difficult to isolate for semi-dilute systems. In this work, we investigate the effect of mixing semiflexible linear chains and rings on the overall clustering behavior in the system. We employ Molecular Dynamics simulations of semiflexible polymers coupled to a solvent modeled by Multi-Particle Collision Dynamics[38,39] without fully-developed hydrodynamic interactions[40,41] and study the impact of steady shear on the system. Varying the chain monomer fraction while keeping the number of monomers constant at three distinct concentrations in the semi-dilute regime, we find that high chain monomer fractions typically

Faculty of Physics, University of Vienna, Boltzmanngasse 5, 1090 Vienna, Austria. E-mail: maximilian.liebetreu@univie.ac.at

make the system behave similarly as it would for pure ring solutions at lower monomer densities. We link this effect to the effective density and topological state of the system, the former decreasing with increasing chain monomer fraction. However, mixing in only a few chains conversely improves clustering behavior as chains get trapped inside of stacks of rings and help stabilizing these structures. Under shear, the investigated properties progressively lose their dependence on chain stoichiometry, converging towards values dictated by monomer density as $\dot{\gamma}$ grows. Not only could this effect be used to improve clustering behavior in ring solutions, it might simultaneously simplify reorientation of clusters in a particular direction using weak shear.

2 Methods

2.1 Numerical model

We perform Molecular Dynamics (MD) simulations to study semiflexible polymers in the bulk under shear. To this end, we employ the Kremer–Grest bead-spring model[42,43] and an additional bending potential to introduce rigidity.[16] The equations of motion are integrated by Velocity-Verlet.[44,45] We use polymer rings of contour length $N_R = 50$ and chains of contour length $N_C = 25$, ensuring that rings and chains, when fully stretched, are of about the same length and still fit inside the simulation box of volume $V = (50 \times 50 \times 50)\sigma^3$ where σ is the length scale of the Lennard-Jones interaction of the Kremer–Grest model. We couple the molecular-dynamics part of the simulation to a solvent modeled by Multi-Particle Collision Dynamics[38,39] (MPCD) with a modification to disable fully-resolved hydrodynamic interactions[40,41] in the interest of computational efficiency. Viscous heating is prevented by employing a Maxwellian cell-level thermostat.[39] Lastly, we employ Lees-Edwards boundary conditions[46] to establish a linear velocity profile corresponding to planar Couette flow such that the expected solvent velocity $\mathbf{v}_s(\mathbf{r}) = \dot{\gamma} y \hat{\mathbf{x}}$, in which $\dot{\gamma}$ is the imposed shear rate, $\mathbf{r} = (x,y,z)$ denotes an arbitrary location, and $\hat{\mathbf{x}}$, $\hat{\mathbf{y}}$, and $\hat{\mathbf{z}}$ indicate flow-, gradient- and vorticity directions.

We use the standard set of MPCD parameters[38,39] corresponding to solvent particle mass $m = 1$, collision angle $\alpha = 130^\circ$, and collision cell side length $a = \sigma$. We set the number of solvent particles per collision cell to $\langle N_c \rangle = 10$ and correspondingly the mass of a polymer bead to $M = m\langle N_c \rangle = 10$. The MPCD timestep was set to $h = 0.1[(k_BT)^{-0.5}m^{0.5}\sigma]$. This combination of parameters creates a solvent with viscosity $\eta_s = 8.70[(k_BT)^{0.5}m^{0.5}\sigma^{-2}]$.

Similarly, we use a well-established set of MD parameters used by Poier *et al.*[16] to study cluster-glass phases of semiflexible rings, as well as in subsequent works on similar systems.[11,24,37] This choice of parameters corresponds to Weaks-Chandler-Andersen potential parameters $\varepsilon = k_BT$ and σ as a unit of length, FENE potential $V_{FENE}(r) = -\varepsilon k R_0^2/\sigma^2 \ln[1 - (r/R_0)^2]$ with spring constant $k = 15k_BT/\varepsilon$ and critical bond extension $R_0 = 1.5\sigma$, and lastly a bending potential acting on consecutive bonds at an angle ϕ to each other: $V_{bend}(\phi) = \varepsilon\kappa_B(1 - \cos(\phi))^2$ with rigidity constant $\kappa_B = 30k_BT/\varepsilon$. For rings in equilibrium at contour length $N_R = 50$, this model yields a radius of gyration of $\langle R_{g,0} \rangle \approx 6.5\sigma$ and an expected bond length of $\langle l_b \rangle = 0.96\sigma$. For chains at contour length $N_C = 25$, one obtains $\langle R_{g,0} \rangle \approx 5.5\sigma$. We employ an MD timestep of $\delta t = 0.002[(k_BT)^{-0.5}m^{0.5}\sigma]$, which is sufficient to prevent concatenation.

2.2 Simulation details

Because of the vast number of monomers in our system and the use of Lees–Edwards boundary conditions,[46] we employ our own custom code written in C++/CUDA[47] to run efficiently on GPUs. This code has been tested extensively and successfully utilized in previous works.[37,48,49] It combines several optimization methods like parallelized MPCD,[50] particle sorting,[51] Verlet- and cell lists,[52] and an adaptation of the cell-list algorithm for Lees–Edwards.[53]

We set the size of our simulation box to $V = (50 \times 50 \times 50)\sigma^3$ and investigate a set of different monomer densities $\rho = N/V = \{0.364, 0.456, 0.600\}\sigma^{-3}$ for monomer counts N. For Fig. 2 and 3 and Fig. 6, we have chosen to use a gray color gradient for $\rho = 0.364\sigma^{-3}$, blue color gradient for $\rho = 0.456\sigma^{-3}$ and a red color gradient for $\rho = 0.6\sigma^{-3}$. Building upon the effective density employed by Bernabei *et al.*[15] and Slimani *et al.*,[25] we define an effective density $\tilde{\rho} = [C_R \cdot \langle V_R \rangle + C_C \cdot \langle V_C \rangle]/V$ where C_X corresponds to ring- (R) or chain (C) count and $\langle V_X \rangle$ to the estimated expected volume of the corresponding objects. Note that $\tilde{\rho}$ always refers to the effective density as measured at equilibrium. Bernabei *et al.*[15] took the cubed equilibrium diameter of gyration $D_{g,0}{}^3$ as a volume estimate. However, in the case of chains, this would severly overestimate the average proximity and overlap of objects in the system. Therefore, as an estimate for these volumes, we instead use the eigenvalues λ_α of the gyration tensor $\hat{G} = 1/N_X \sum_{i=1}^{N_X} \mathbf{s}_i \otimes \mathbf{s}_i{}^1$ (where $\otimes$ is the dyadic product and $\mathbf{s}_i$ is the vector from the object's center-of-mass to the position of particle i) such that $\langle V_X \rangle = \langle \lambda_1 \rangle \cdot \langle \lambda_2 \rangle \cdot \langle \lambda_3 \rangle$. We further define the chain monomer fraction as $Q_{CR} = C_C N_C/N$, *i.e.*, the fraction of number of monomers belonging to chains, $C_C N_C$, to the total number N of monomers in the system. Accordingly, low values of Q_{CR} indicate a system dominated by rings. The effective equilibrium densities $\tilde{\rho}$ for different values of ρ and Q_{CR} can be found in Table 1 below.

We follow the method set forth by Bernabei *et al.*[15] and employed as well in subsequent works[16,25] to identify stacks of rings. To this end, we define the director $\mathbf{d}_i$ of a ring i to be equivalent to the eigenvector corresponding to the smallest

Table 1 Effective equilibrium densities $\tilde{\rho}$ for a variety of different chain monomer fractions Q_{CR} and monomer densities ρ

Q_{CR}	$\tilde{\rho}$ ($\rho = 0.364\sigma^{-3}$)	$\tilde{\rho}$ ($\rho = 0.456\sigma^{-3}$)	$\tilde{\rho}$ ($\rho = 0.600\sigma^{-3}$)
0.00	3.00	3.66	4.72
0.10	2.60	3.14	3.96
0.25	2.49	2.77	3.16
0.50	1.77	2.24	2.44
0.75	1.19	1.50	1.79
0.90	0.78	0.92	1.24
1.00	0.44	0.56	0.71

eigenvalue of the gyration tensor $\hat{G}$. As such, $\mathbf{d}_i$ is always perpendicular to the plane in which the open semiflexible ring resides. We can then employ the following criteria for deciding whether any ring i is on the same stack as a ring j:

$$\begin{aligned} \| \mathbf{d}_i \cdot \mathbf{d}_j \| &\geq 1 - \Delta\gamma \\ \| \mathbf{r}_{ij} \cdot \mathbf{d}_i \| &\leq v_{\|} \\ \| \mathbf{r}_{ij} - \mathbf{d}_i \cdot (\mathbf{r}_{ij} \cdot \mathbf{d}_i) \| &\leq v_{\perp} \end{aligned} \quad (1)$$

in which $\mathbf{r}_{ij}$ is the distance vector between the rings' centers-of-mass, and $\Delta\gamma = 0.1$, $v_{\|} = 3.0\sigma$ and $v_{\perp} = 2.5\sigma$ are parameters chosen *a posteriori* to identify stacks in agreement with visual intuition. The results are qualitatively robust with respect to small variations in these parameters. Because this kind of ordering is unique to semiflexible rings, we omit chains from this consideration.

We prepare our mixtures by taking a fully equilibrated system of rings in the cluster-glass phase, cutting random rings open, and allowing the system to equilibrate again. The same initial equilibrated pure-ring system was used for preparing all simulations, and the same initial equilibrated ring-chain mixtures were used for varying shear rates $\dot{\gamma}$ at constant chain monomer fraction Q_{CR} to enable highlighting of shear and chain fraction, and maintaining system comparability. We define the Weissenberg number[54] $Wi_0 = \dot{\gamma} \cdot \tau_{R,0}$, a quantity computed from shear rate $\dot{\gamma}$ and relaxation time $\tau_{R,0}$ of a semiflexible ring in dilute solution in equilibrium. We then simulate each system for about $t = 3 \times 10^6 [(k_B T)^{-0.5} m^{0.5} \sigma]$, with the exact number varying slightly due to runtime restrictions on the employed GPU cluster. By fitting the autocorrelation function $\Phi(t)$ of the end-to-end vector for chains and the maximum-distance vector between beads i and $i + N_R/2$ for rings with $f(t) = a_0 e^{-t/\tau_1} + (1 - a_0) e^{-t/\tau_2}$, we obtain $\tau_R = \int_0^\infty f(t) \mathrm{d}t$.[55] We determine the dilute-equilibrium relaxation times $\tau_{R,0} \cong 62\,000 [(k_B T)^{-0.5} m^{0.5} \sigma]$ for the chains and $\tau_{R,0} \cong 46\,000 [(k_B T)^{-0.5} m^{0.5} \sigma]$ for our rings.

3 Results and discussion

3.1 Ring clustering behavior in ring-chain mixtures

Semiflexible rings in concentrated solutions in equilibrium exhibit clustering behavior and self-organize into stacks.[15,16,24,25] Under sufficiently weak shear, these stacks reorient and align with the flow direction.[37] In this work, we demonstrate the changes introduced by mixing chains and rings into the same system. Specifically, we cut open some of the rings, thus keeping the monomer density ρ constant.

First, we look at the centers-of-mass of the polymers in our system to obtain an overall view of the ensuing phenomenon after imposing shear. In Fig. 1, we show centers-of-mass of rings (red) and chains (blue) for Wi_0 spanning four orders of magnitude and Q_{CR} between 0.0 and 0.5 with $\rho = 0.6\sigma^{-3}$. At equilibrium, the rings in the system look equally as organized into clusters at $Q_{CR} = \{0.0, 0.1, 0.25\}$, whereas shorter clusters can be discerned at $Q_{CR} = 0.5$. As Wi_0 increases, stacks begin to align with the flow.[37] At $Wi_0 = 0.04552$, we observe regular alignment for $Q_{CR} = \{0.0, 0.1\}$, similarly pronounced alignment for $Q_{CR} = 0.25$ and clusters already breaking for $Q_{CR} \geq 0.5$. At $Wi_0 = 0.45524$, stacks are fully aligned for $Q_{CR} = \{0.0, 0.1\}$, start dissembling for $Q_{CR} = 0.25$ and are mostly broken for $Q_{CR} \geq 0.5$. As Wi_0 is increased another order of magnitude, very few and only short clusters can be seen independent of Q_{CR}.

Intuitively, we expect that low values of Q_{CR} would yield similar results to a pure-ring solution or even slightly improve clustering. Additionally, it seems that higher values of Q_{CR} might cause clusters to align and eventually also dissemble at comparatively lower Wi_0. Increasing Q_{CR} past $Q_{CR} \cong 0.25$ severely reduces clustering in the system when compared to lower Q_{CR} values.

We can verify and quantify this behavior using the dispersion index DI of the centers-of-mass of our rings and chains as described by Kam *et al.*[57] and also Liebetreu and Likos;[37] this quantity is shown in Fig. 2a and b. To this end, we introduce a cubic grid of cell length $l = 2.5\sigma$ and measure sample mean μ of the number of centers-of-mass per cell. We label the sample standard deviation of this quantity s. The dispersion index DI is then calculated as $\mathrm{DI} = s^2/\mu$. Characteristically, a value of DI = 1 indicates a random arrangement of centers-of-mass in accordance with a Poisson distribution. Values of DI < 1 point at more-than-random uniformity, for example grid-like symmetry for all individual centers-of-mass, whereas DI > 1 signifies clustering. It should be noted that the justification for employing this parameter is mostly a comparative one. In Fig. 2c, we provide the probability $p(h_c > 5)$ for a ring to belong to a stack with more than 5 members, which produces a similar graph. The advantage of DI, however, is that the choice of 5 members for $p(h_c > 5)$ is arbitrary and not necessarily indicative of clustering. Moreover, removing rings from a given system can drastically alter $p(h_c > 5)$, while DI should be more robust under such changes and provide a more robust measure for clustering when altering Q_{CR}. In addition, the dispersion index DI always has a reference value of 1 to indicate clustering or uniformity in the system.

Fig. 2 shows the dispersion index DI both for chains (Fig. 2a) and for rings (Fig. 2b). DI for chains is, across shear rates and effective densities $\tilde{\rho}$, at around DI $\lesssim 1$. A notable exception occurs for the most concentrated solution $\rho = 0.6\sigma^{-3}$ at $Q_{CR} = \{0.1, 0.25\}$, where chains appear to exhibit some weak clustering behavior following the strong clustering of the rings in that system. Curiously, this exception is also visible in Fig. 2b for the rings, where equilibrium values of DI at $Q_{CR} = \{0.1, 0.25\}$ exceed DI at $Q_{CR} = 0$. A similar effect can be discerned at $Q_{CR} = 0.1$ for semi-concentrated solutions at $\rho = 0.456\sigma^{-3}$, whereas it vanishes for the most dilute concentration investigated, $\rho = 0.364\sigma^{-3}$. Looking at the effective densities $\tilde{\rho}$, the effect is visible where $\tilde{\rho} \gtrsim 3.0$ (compare Table 1), which we will therefore treat as an estimate for a stabilization threshold in this context. This threshold is also discussed later in the context of Fig. 7 for momentary effective densities $\tilde{\rho}_m$, where these transitions are shown to be linked to $\tilde{\rho}_m$, but also influenced by Q_{CR} and, subsequently, topology.

The weak clustering of the chains could point at chains becoming trapped inside or between clusters of rings – an

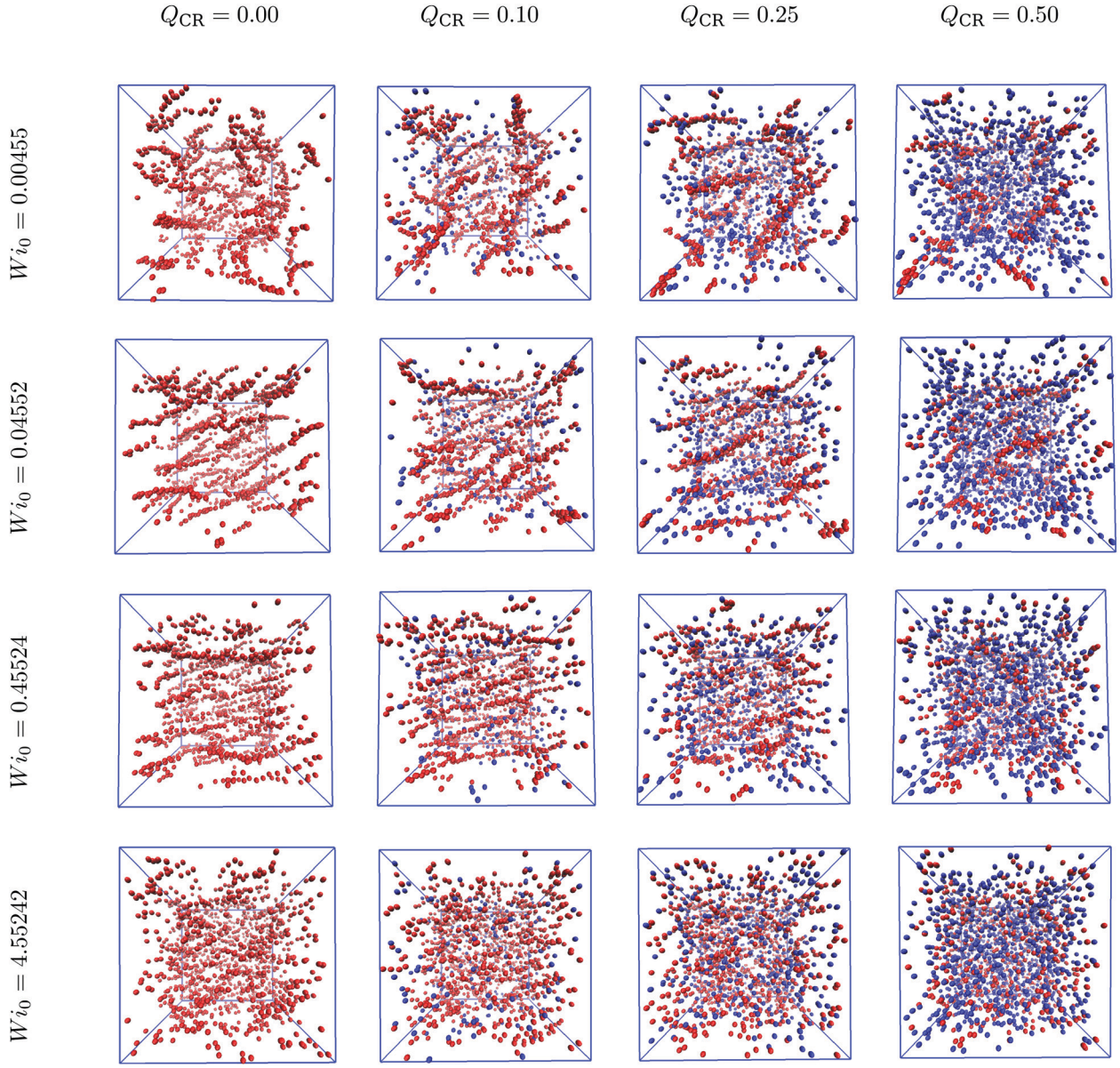

Fig. 1 Cluster phase in chain-ring mixtures. Centers-of-mass of rings (red) and chains (blue) for a variety of different Weissenberg numbers Wi_0 and chain monomer fractions Q_{CR}. The simulation box is shown in blue, and the system is projected onto the flow-gradient plane. The snapshots were created using VMD,[56] and the corresponding monomer density is $\rho = 0.6\sigma^{-3}$. Left to right: Increasing chain monomer fraction Q_{CR} at constant Weissenberg number Wi_0. Top to bottom: Increasing Weissenberg number Wi_0 at constant chain monomer fraction Q_{CR}.

observation difficult to quantify, but one which agrees well with our visual impression of the system from Fig. 1. It seems plausible that this trapping could potentially stabilize the clusters under shear, protecting them from breaking into smaller clusters even at high shear rates, but we do not observe such an effect. In fact, for increasing shear, the same behavior can be seen for all the investigated systems: DI decreases with shear, and ultimately, DI for rings starts to converge against DI $\cong 1$ independent of $\tilde{\rho}$ or Q_{CR}. It appears the chains in this work, at least, are either too short or too rigid to effectively tangle the rings and hold them in place. However, small non-zero values of Q_{CR} seem to at least improve clustering behavior in equilibrium, and they do not appear to influence the slope of DI as shear increases, given $\tilde{\rho} \gtrsim 3.0$ (compare Table 1).

Finally, we plot the probability $p(h_c > 5)$ for a randomly-selected ring to be part of a stack with a ring count $h_c > 5$ in Fig. 2c. Unsurprisingly, this probability decreases consistently with increasing shear as clusters start to break apart. Curiously, at $\rho = \{0.456, 0.6\}\sigma^{-3}$, low values of Q_{CR} cause well-separated graphs at high shear and overlapping graphs near equilibrium, even though there are less rings in the system as Q_{CR} increases.

This provides further evidence that a small amount of chains can enhance cluster formation, or at the very least does not disrupt it. The observed improvement is, however, small, and we cannot confirm without reasonable doubt that the effect is not just the result of some noise. On the other hand, the consistent behavior across different densities ρ for values of

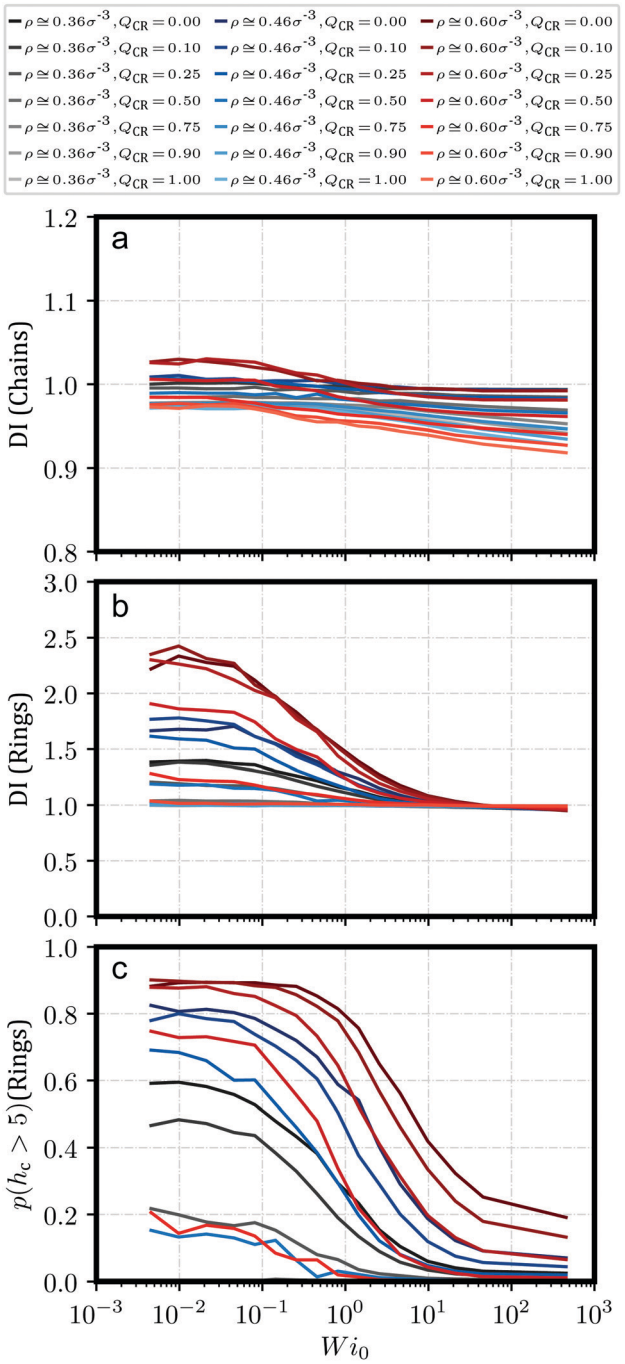

Fig. 2 Quantitative indicators for clustering against Weissenberg number Wi_0 for a variety of different monomer densities ρ and chain monomer fractions Q_{CR}. (a) dispersion index DI, only chains. (b) dispersion index DI, only rings. Values of DI > 1 indicate clustering. (c) probability $p(h_c > 5)$ for a ring to belong to a stack with more than 5 members. Higher probabilities indicate clustering.

$Q_{CR} = \{0.0, 0.1\}$ and the unchanging values obtained for $p(h_c > 5)$ at low values of Wi as shown in Fig. 2c indicate that future investigations of the system at these parameters might provide further evidence for the effect discussed here, and potentially show that clustering is not just equal but stronger under the addition of a few chains at $Q_{CR} \cong 0.1$, at least for sufficient overall densities ρ.

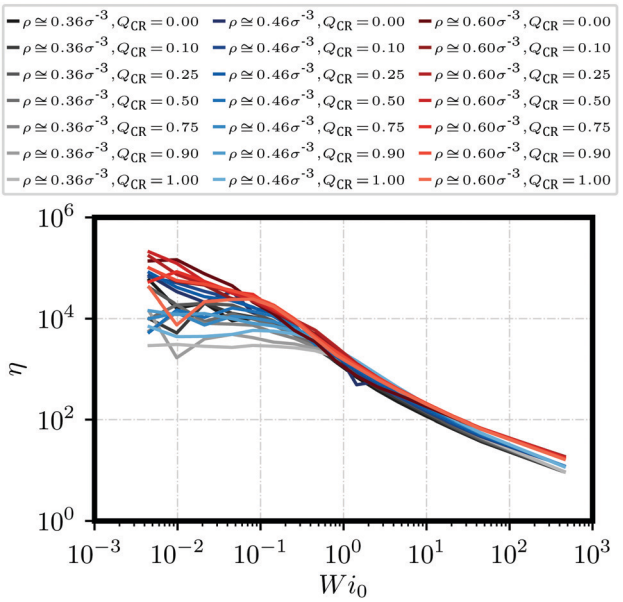

Fig. 3 Polymeric viscosity η against Weissenberg number Wi_0 for a variety of different monomer densities ρ and chain monomer fractions Q_{CR}.

Next, we look at the rheological properties of the system through the polymeric viscosity[58] $\eta = -\sigma_{xy}/\dot{\gamma}$ where σ_{xy} is the flow-gradient element of the stress tensor as computed from the modified Kramers expression[59] $\sigma_{xy} = \sum_{i=1}^{N} \langle \mathbf{s}_{i,x} \mathbf{f}_{i,y} \rangle$ where $\mathbf{f}_i$ is the total force acting on bead i. We have already established from Fig. 2 that the chains in this work do not effectively tangle the rings to keep them on formed clusters as shear increases. Fig. 3 confirms this effect through clear shear-thinning qualitatively independent of $\tilde{\rho}$ and Q_{CR}. We suggest that both the rigidity of the chains and their shortness might be detrimental to shear thickening, with some chains getting trapped within the stacks, but then aligning with them or simply capable of escaping a given stack without causing too much friction.

We establish a direct correlation between polymeric viscosity η and monomer density ρ, highlighted by three distinct bands at high shear in Fig. 3. This also indicates that any topological influence becomes drastically reduced at high shear, and that the main factor for polymeric viscosity in this regime is the monomer density ρ rather than the effective density $\tilde{\rho}$ or the chain monomer fraction Q_{CR}. Across all investigated mixtures, there seems to be a shear regime in which low values of Q_{CR} lead to lower relative viscosities η when compared to graphs of higher Q_{CR} at equal ρ. Unfortunately, the effect is difficult to see and more difficult to isolate. We suggest this occurs because, as clusters are broken apart by shear, chains might cause additional friction and align at a different rate than rings. We will revisit this question in Section 3.3.

3.2 Stack orientation under shear

We have defined the director $\mathbf{d}$ of a ring as its plane normal, computed from the eigenvector of its gyration tensor $\hat{G}$ corresponding to its smallest eigenvalue. The clusters formed under

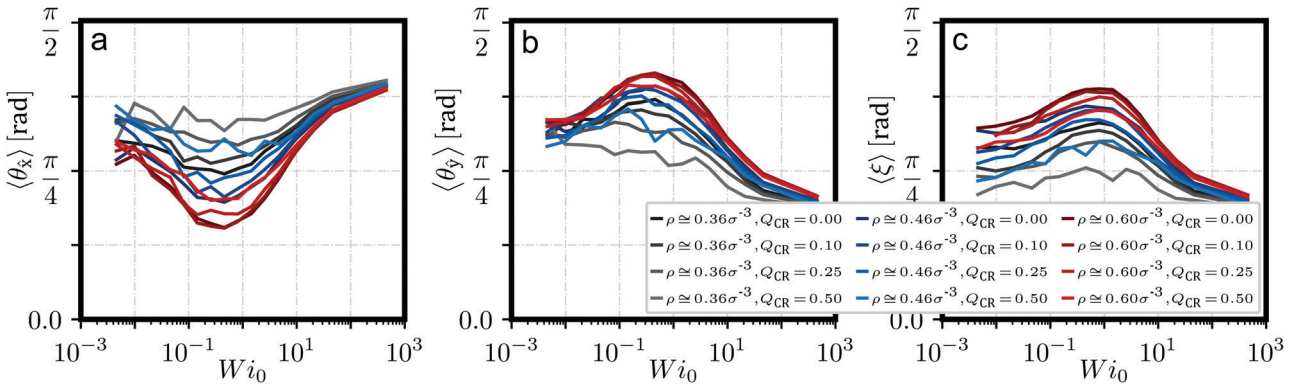

Fig. 4 Stack orientation. Several angles describing the orientation of stacks with a stack size of $h_c > 5$ both with respect to flow but also to individual rings against Weissenberg number Wi_0 for $Q_{CR} \in [0.0, 0.5]$ and different monomer densities ρ. (a) Angle $\langle\theta_{\hat{\mathbf{x}}}\rangle$ between main cluster axis and flow axis $\hat{\mathbf{x}}$. (b) Angle $\langle\theta_{\hat{\mathbf{y}}}\rangle$ between main cluster axis and gradient axis $\hat{\mathbf{y}}$. (c) Angle $\langle\xi\rangle$, expressing the average angle between main cluster axis and the directors **d** of all rings on that cluster.

equilibrium are typically oriented randomly. Under shear, those stacks start to align themselves with flow until they eventually break apart.[37] We show quantitative evidence of this phenomenon in Fig. 4, which describes angles $\langle\theta_{\hat{\mathbf{x}}}\rangle$ of stack axis to flow, $\langle\theta_{\hat{\mathbf{y}}}\rangle$ of stack axis to gradient and $\langle\xi\rangle$ of stack axis to individual ring directors **d**. The stack axis is computed as the main principle component *via* $\hat{G}$ of the set of centers-of-mass of rings on that stack.

An important feature of these angles is that they show the alignment of stacks as shear increases, up to about $Wi_0 \cong 0.5$, where we find a minimum for $\langle\theta_{\hat{\mathbf{x}}}\rangle$ in Fig. 4a. For $Wi_0 \gtrsim 0.5$, clusters break apart and long aggregates become increasingly unlikely. Another indicator for this behavior is $p(h_c > 5)$ in Fig. 2c, which shows a rapid decline for $Wi_0 \gtrsim 0.5$ across all values of $\tilde{\rho}$ and Q_{CR}. If one compares $\langle\theta_{\hat{\mathbf{y}}}\rangle$ to $\langle\xi\rangle$ in Fig. 4b and c, one can see $\langle\xi\rangle$ mimicking the behavior of $\langle\theta_{\hat{\mathbf{y}}}\rangle$ shifted to slightly higher values of Wi_0. We suggest that stacks, which are expected to have a much higher relaxation time than individual rings, respond to shear before individual rings do, thus causing stacks to align even as rings still maintain their equilibrium orientations. Only at higher shear rates, when rings start to align as well, do the clusters break apart.

The observed alignment effect with shear becomes less pronounced for higher values of Q_{CR} across all investigated monomer densities ρ. We suggest that this is simply due to less and shorter clusters forming under such conditions as chains become increasingly system-dominating, an observation taken from Fig. 2. Such short clusters can also be detected as a side effect of the employed algorithm for detecting these stacks when rings in the system become increasingly aligned in the same way and happen to pass each other. This effect becomes increasingly pronounced at high shear and directly influences the angles as seen here. For high values of Q_{CR}, the system is dominated by chains, and the few clusters which might form will be increasingly short and short-lived, showing this side-effect even close to equilibrium.

In the context of chains potentially helping the alignment of clusters under shear, no such effect can be discerned here. At $Q_{CR} = \{0.1, 0.25\}$, the graphs for $\rho = 0.6\sigma^{-3}$ are almost indistinguishable, so we can conclude that the addition of only a few chains does not significantly alter the alignment of stacks under shear. Overall, the alignment here seems to follow similar rules for when chain monomer fractions start affecting the system as we described before from Fig. 2.

3.3 Individual chains and rings in the mixture

We visualize some typical configurations of rings (red) and chains (blue) in the aforementioned simulations at $Q_{CR} = \{0.1, 0.25\}$ in Fig. 5. One can identify the alignment of both rings and chains as shear increases, as well as spot the onset of twisting for rings, which is more pronounced for still higher values of the shear rate.[37] Chains instead exhibit stretching. Tumbling, which occurs for both chains and rings in these simulations, is difficult to visualize from snapshots. It should be noted that here, we can even see a more complete alignment of rings into the flow-vorticity plane for $Wi_0 = 0.45524$ and $Q_{CR} = 0.25$ when compared to $Q_{CR} = 0.10$ at equal Wi_0, as well as the onset of stack destruction as shown in Fig. 1 and 2. This observation provides further evidence that as rings align with the flow, clusters start breaking. At constant monomer density ρ, increasing the chain monomer fraction Q_{CR} means creating a more chain-dominated system in which the remaining rings have more space to orient themselves ($\tilde{\rho}$ will be lower if ρ is kept constant).

In Fig. 6, we present instructive properties of individual chains and rings. First, we define the radius of gyration $\langle R_g\rangle = \langle\sqrt{\lambda_1 + \lambda_2 + \lambda_3}\rangle$ for eigenvalues $\lambda_1 \geq \lambda_2 \geq \lambda_3$ of the gyration tensor $\hat{G}$[1,60] and visualize it in Fig. 6a and d. Its value typically scales proportional to effective density $\tilde{\rho}$. Semiflexible chains exhibit swelling under shear as they stretch and elongate up to a maximum value, then deflate as shear increases further due to tumbling (Fig. 6a). Rings do not exhibit swelling; their rigidity causes them to not stretch enough to balance out a twisting which is entropically favorable to stretching. Instead, rings deflate under shear (Fig. 6d). However, this twisting nevertheless makes them resemble a prolate object, and their form mimicks that of the chains in strong shear.

To quantify this behavior, we define the prolateness S^* which inhibits values from -0.25 (a circle) to 2 (a straight line)

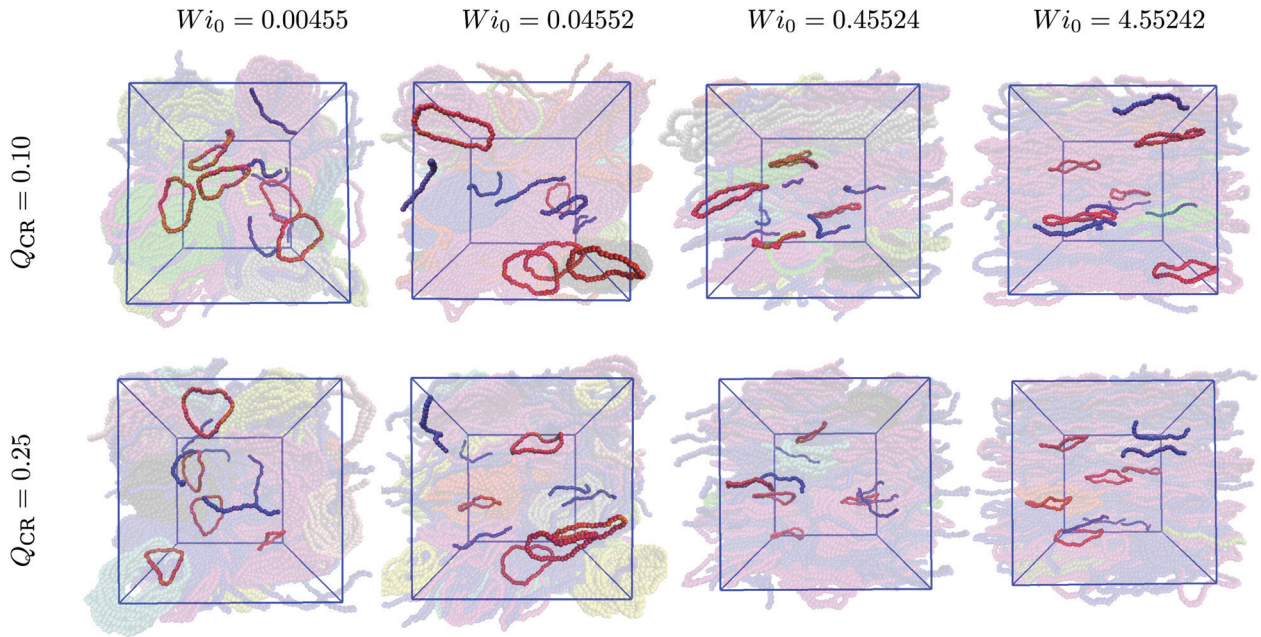

Fig. 5 Typical ring- and chain configurations. Some select chains (blue) and rings (red) are highlighted for a variety of Weissenberg numbers Wi_0 and two chain monomer fractions Q_{CR} = {0.1, 0.25} to show their typical conformations. Simulation boxes are drawn in blue as seen in the flow-gradient plane. Left to right: Increasing Weissenberg number Wi_0 at constant chain monomer fraction Q_{CR} and monomer density $\rho = 0.6\sigma^{-3}$. Top to bottom: Increasing chain monomer fraction Q_{CR} from 0.1 to 0.25 at constant Weissenberg number Wi_0.

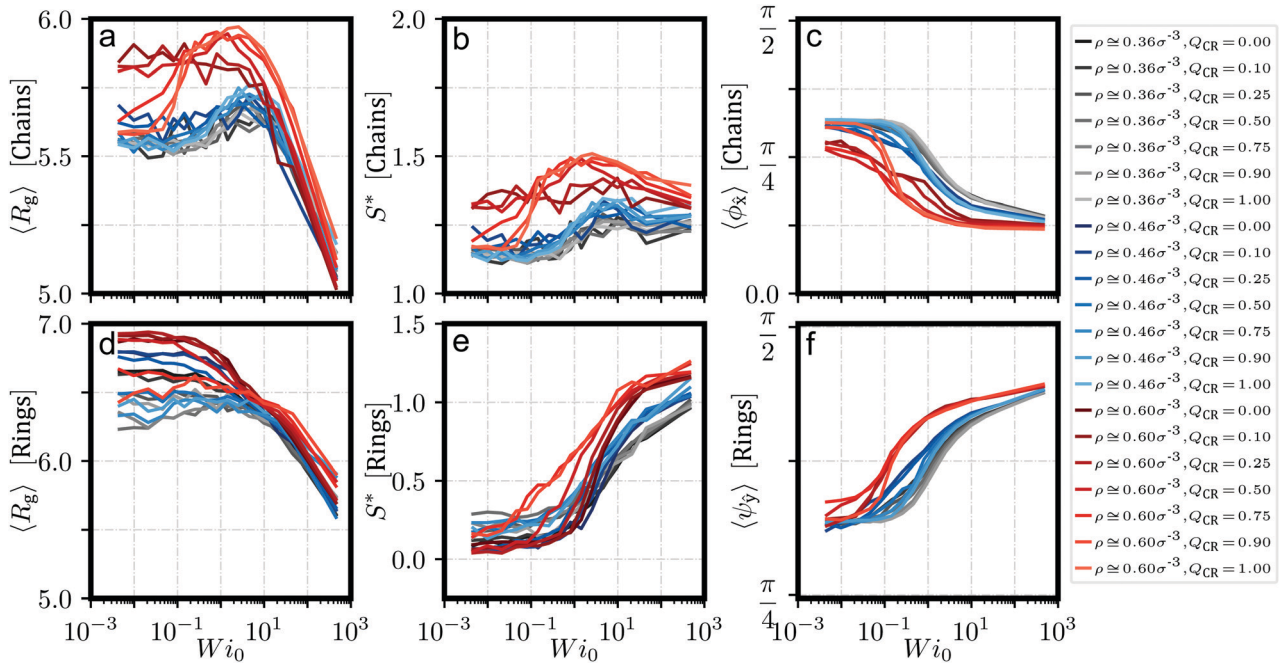

Fig. 6 Shape parameters for chains and rings scaling with Weissenberg number Wi_0 and for different chain monomer fractions Q_{CR} and monomer densities ρ. (a–c) Chains. (d–f) Rings. (a and d) Gyration radius $\langle R_g \rangle$. (b and e) Prolateness $S^* \in [-0.25, 2.0]$. (c) Angle $\langle \phi_{\hat{x}} \rangle$, indicating angle between main principal component of chain and flow axis. (f) Angle $\langle \psi_{\hat{y}} \rangle$, indicating angle between ring director d and gradient axis.

and describes how ellipsoidal a shape is. *Via* the eigenvalues λ_i of $\hat{G}$, S^* can be computed in the following fashion:[1,60]

$$S^* = \left\langle \frac{(3\lambda_1 - R_g^2)(3\lambda_2 - R_g^2)(3\lambda_3 - R_g^2)}{R_g^6} \right\rangle, \qquad (2)$$

and we present the result in Fig. 6b for chains and Fig. 6e for rings. While semiflexible chains resemble a straight line almost independently of shear rate, rings, especially at high monomer densities, twist themselves into a shape that more and more resembles that of the linear chain. This also provides an explanation

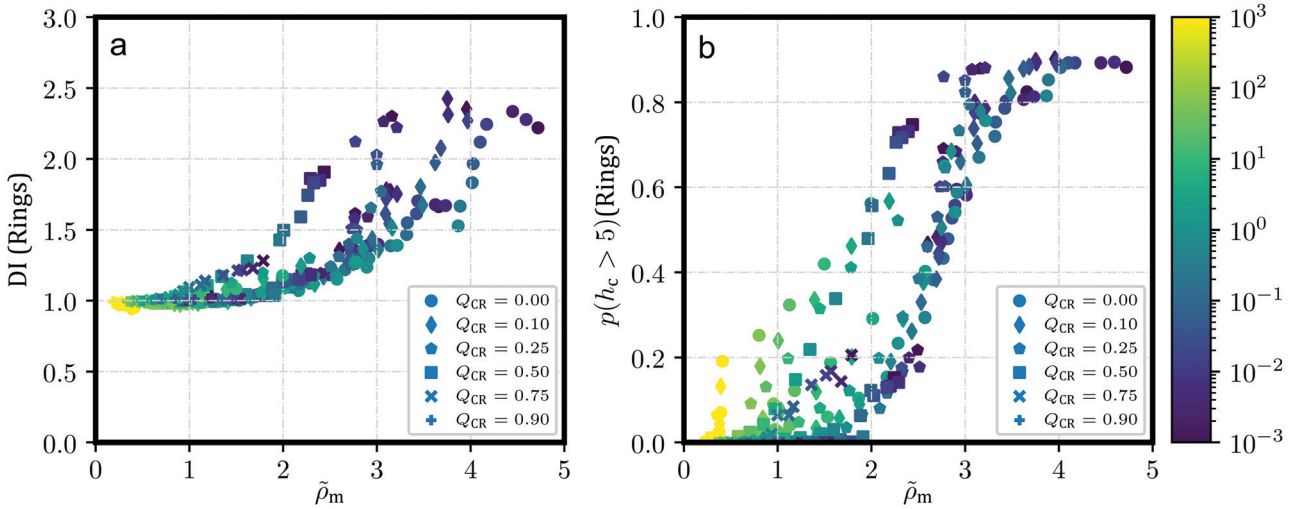

Fig. 7 Influence of effective densities on clustering. Scatterplots for dispersion index DI and $p(h_c)$ against momentary effective density $\tilde{\rho}_m$ from all investigated shear rates, monomer densities and chain monomer fractions. Markers indicate values of Q_{CR} as shown in the legend; colors indicate values of Wi_0 as shown in the color bar. (a) Dispersion index DI against $\tilde{\rho}_m$. (b) $p(h_c)$ against $\tilde{\rho}_m$.

for the viscosity in Fig. 3 – at high shear, rings and chains offer little difference in shape, and thus, monomer density becomes the defining factor in that regime.

We confirm from Fig. 6c and f that chains align themselves with the flow axis while rings align themselves into the flow-vorticity plane, which confirms our observations from Fig. 5. Note that we are measuring angles to an axis, so we are biasing our values away from perfect alignment.

We finally turn our attention to the question of the impact of the effective density $\tilde{\rho}$ on clustering behavior, which is summarized in Fig. 7. The main question here is whether the clustering behavior discussed around the findings presented in Fig. 2 is mainly dictated by effective density $\tilde{\rho}$ rather than by the topological effects introduced by mixing chains and rings. To this end, we define the momentary effective density $\tilde{\rho}_m$, similarly to the effective density $\tilde{\rho}$, with the volume computed from averaged gyration tensor eigenvalues $\langle\lambda_i\rangle$ not at equilibrium, but instead in any given mixture at $Wi_0 > 0$.

As the shear rate and the chain monomer fraction Q_{CR} increase, the quantity $\tilde{\rho}_m$ decreases accordingly because rings and chains stretch and deform, reducing thereby the volumes of the ellipsoids of inertia $\langle V_C\rangle$ and $\langle V_R\rangle$. The values scanned by the quantity $\tilde{\rho}_m$ in mixtures across varying Wi_0, ρ and Q_{CR} lie in the same range, independently of the details of the mixture stoichiometry. If the topological differences between chains and rings were negligible and instead their different sizes caused the phenomena discussed in this work, then we should see all values of DI and $p(h_c)$ in Fig. 7 collapse onto a single graph, respectively. This is clearly not the case here, therefore topology is important.

There are other possibilities: if the different clustering strengths are tied only to monomer densities ρ and topological differences had no effect, we should see three distinct graphs each showing slightly different dependence on $\tilde{\rho}_m$. This could apply here at least in parts of the figure, but it is not an exhaustive explanation. Besides, we have already established that clustering is stronger for high values of ρ, so this influence is not surprising. Alternatively, if Q_{CR} was the sole driving force behind clustering strength, we should see the same markers at the same values for DI and $p(h_c)$ for varying $\tilde{\rho}_m$, respectively. This is not the case here, either.

Similarly, we can get another indication for the decreasing significance of topology for high values of Wi_0: this is easiest to see in Fig. 7a where we find overlapping same-colored data points at the lowest exhibited values of $\tilde{\rho}_m$, meaning that at these shear rates, $\tilde{\rho}_m$ is almost the same independent of Q_{CR}. Here, we see overlapping datapoints only in the high-shear regime, and the same markers are not always found at the same values of DI or $p(h_c)$. It is no surprise that ρ would be the main driving force behind clustering strength - this has already been established in Fig. 2. However, on top of this, we show here that Q_{CR} has a significant impact of its own on clustering behavior in the system, one that is not only caused by the difference in $\tilde{\rho}_m$, especially for moderate shear $Wi_0 \in [10^{-1}, 10^{1}]$. Again, if that were the case and the topological difference had less impact than the difference in size, we should see the scatterplots collapse onto single graphs such that the quantities shown in Fig. 7 would depend only on $\tilde{\rho}_m$, which is not the case.

Close to equilibrium, momentary effective densities $\tilde{\rho}_m$ are heavily influenced by Q_{CR} as shapes are distinctly different, but at least for $Q_{CR} \in [0.0, 0.25]$, the impact on clustering is negligible, confirming our previous observations about mixing in chains and the parameter regimes in which it impacts the system the strongest. Most importantly, we can discern distinct graphs, meaning that even at same initial effective densities, different clustering behavior can be achieved by varying Q_{CR}.

4 Conclusions

In this work, we have investigated the effect of cutting open semiflexible rings in a concentrated solution to create a

chain-ring mixture. We have denoted the chain monomer fraction as Q_{CR}. We find that small values of Q_{CR} do not significantly alter the clustering- and general behavior of the solvent, and values $Q_{CR} \gtrsim 0.5$ make clustering progressively unlikely. Under weak shear, the addition of chains alters neither clustering behavior nor cluster alignment. However, the addition of chains does significantly alter the effective densities $\tilde{\rho}$ observed in the system. For high Weissenberg numbers Wi_0, topological influences become negligible as both chains and rings become highly elongated and tumble. In this regime, monomer density ρ takes precedence over Q_{CR} or $\tilde{\rho}$.

Initially, chains might get trapped within clusters, but their length is not sufficient to entangle the stacks, and under shear, the stacks break apart using the same mechanism as described before.[37] We find that the addition of a small number of chains into a system of semiflexible rings (low values of Q_{CR}) does not appear to affect the clustering behavior of the system, neither with nor without shear. Therefore, experimental investigation of such systems should not require polymer blends that only, exclusively, feature rings.

Future work in this direction should investigate especially the regime of $Q_{CR} \in [0.0, 0.25]$ and $Wi_0 \in [10^{-3}, 10^{0}]$ in which chains might aid the system in clustering. Of particular interest will be the variation of rigidity, either in general or only for the chains to increase the overall entanglement in the system. For this subset of shear rates and chain monomer fractions, additional investigations could also alter chain contour length. It is possible that, for chains of the same contour length as the rings, their effect on clustering behavior might be much stronger, and we encourage the tools developed and presented in this work be applied to further, similar investigations.

Conflicts of interest

There are no conflicts to declare.

Acknowledgements

The computational results presented have been achieved in part using the Vienna Scientific Cluster (VSC). M. L. has been supported by the uni:docs Doctoral Fellowship Programme of the University of Vienna.

Notes and references

1 J. Aronovitz and D. Nelson, *J. Phys.*, 1986, **47**, 1445–1456.
2 A. Y. Grosberg, A. Feigel and Y. Rabin, *Phys. Rev. E: Stat. Phys., Plasmas, Fluids, Relat. Interdiscip. Top.*, 1996, **54**, 6618–6622.
3 S. S. Jang, T. Çağin and W. A. Goddard, *J. Chem. Phys.*, 2003, **119**, 1843–1854.
4 N. T. Moore, R. C. Lua and A. Y. Grosberg, *Proc. Natl. Acad. Sci. U. S. A.*, 2004, **101**, 13431–13435.
5 A. Narros, A. J. Moreno and C. N. Likos, *Macromolecules*, 2013, **46**, 3654–3668.
6 A. Prhashanna, S. Khan and S. Chen, *Colloids Surf., A*, 2016, **506**, 457–466, DOI: 10.1016/j.colsurfa.2016.07.003.
7 T. Yamamoto and N. Masaoka, *Rheol. Acta*, 2015, **54**, 139–147.
8 L. Weiss, A. Nikoubashman and C. N. Likos, *ACS Macro Lett.*, 2017, **6**, 1426–1431.
9 S. F. Edwards, *Proc. Phys. Soc.*, 1967, **91**, 513–519.
10 S. F. Edwards, *J. Phys. A*, 1968, **1**, 15–28.
11 P. Poier, S. A. Egorov, C. N. Likos and R. Blaak, *Soft Matter*, 2016, **12**, 7983–7994.
12 L. B. Weiss, C. N. Likos and A. Nikoubashman, *Macromolecules*, 2019, **52**, 7858–7869.
13 D. Vlassopoulos, T. Pakula, G. Fytas, J. Roovers, K. Karatasos and N. Hadjichristidis, *Europhys. Lett.*, 1997, **39**, 617–622.
14 A. Y. Grosberg, *Soft Matter*, 2014, **10**, 560–565.
15 M. Bernabei, P. Bacova, A. J. Moreno, A. Narros and C. N. Likos, *Soft Matter*, 2013, **9**, 1287–1300.
16 P. Poier, C. N. Likos, A. J. Moreno and R. Blaak, *Macromolecules*, 2015, **48**, 4983–4997.
17 A. R. Klotz, B. W. Soh and P. S. Doyle, *Proc. Natl. Acad. Sci. U. S. A.*, 2020, **117**, 121–127.
18 Y. Arai, R. Yashuda, K. Akashi, Y. Harada, H. Miyata, K. Kinoshita Jr. and H. Itoh, *Nature*, 1999, **399**, 446–448.
19 L. Hu, C.-H. Lu and I. Willner, *Nano Lett.*, 2015, **15**, 2099–2103.
20 C.-H. Lu, A. Cecconello, X.-J. Qi, N. Wu, S.-S. Jester, M. Famulok, M. Matthies, T.-L. Schmidt and I. Willner, *Nano Lett.*, 2015, **15**, 7133–7173.
21 C.-H. Lu, A. Cecconello and I. Willner, *J. Am. Chem. Soc.*, 2016, **138**, 5172–5185.
22 Z. Ahmadian, I. Chubak, C. N. Likos and M. R. Ejtehadi, *Soft Matter*, 2020, **16**, 3029–3038, DOI: 10.1039/c9sm02374g.
23 P. M. Rauscher, K. S. Schweizer, S. J. Rowan and J. J. de Pablo, *Macromolecules*, 2020, **53**, 3390–3408.
24 P. Poier, P. Bacová, A. J. Moreno, C. N. Likos and R. Blaak, *Soft Matter*, 2016, **12**, 4805–4820.
25 M. Z. Slimani, P. Bacova, M. Bernabei, A. Narros, C. N. Likos and A. J. Moreno, *ACS Macro Lett.*, 2014, **3**, 611–616.
26 A. Moreno and C. N. Likos, *Phys. Rev. Lett.*, 2007, **99**, 107801.
27 D. G. Tsalikis and V. G. Mavrantzas, *ACS Macro Lett.*, 2014, **3**, 763–766.
28 D. G. Tsalikis, V. G. Mavrantzas and D. Vlassopoulos, *ACS Macro Lett.*, 2016, **5**, 755–760.
29 S. Goossen, M. Krutyeva, M. Sharp, A. Feoktystov, J. Allgaier, W. Pyckhout-Hintzen, A. Wischnewski and D. Richter, *Phys. Rev. Lett.*, 2015, **115**, 148302.
30 D. Vlassopoulos, *Rheol. Acta*, 2016, **55**, 613–632.
31 G. D. Papadopoulos, D. G. Tsalikis and V. G. Mavrantzas, *Polymers*, 2016, **8**, 283.
32 D. G. Tsalikis, P. V. Alatas, L. D. Peristeras and V. G. Mavrantzas, *ACS Macro Lett.*, 2018, **7**, 916–920.
33 M. Kruteva, J. Allgaier and D. Richter, *Macromolecules*, 2017, **50**, 9482–9493.
34 J. D. Halverson, W. B. Lee, G. S. Grest, A. Y. Grosberg and K. Kremer, *J. Chem. Phys.*, 2011, **134**, 204904.
35 J. D. Halverson, W. B. Lee, G. S. Grest, A. Y. Grosberg and K. Kremer, *J. Chem. Phys.*, 2011, **134**, 204905.
36 J. D. Halverson, G. S. Grest, A. Y. Grosberg and K. Kremer, *Phys. Rev. Lett.*, 2012, **108**, 038301.

37 M. Liebetreu and C. N. Likos, *ACS Appl. Polym. Mater.*, 2020, **2**(8), 3505–3517, DOI: 10.1021/acsapm.0c00522.
38 A. Malevanets and R. Kapral, *J. Chem. Phys.*, 1999, **110**, 8605–8613.
39 G. Gompper, T. Ihle, D. Kroll and R. Winkler, *Adv. Polym. Sci.*, 2008, **221**, 1–91.
40 N. Kikuchi, A. Gent and J. M. Yeomans, *Eur. Phys. J. E*, 2002, **9**, 63–66.
41 M. Ripoll, R. G. Winkler and G. Gompper, *Eur. Phys. J. E*, 2007, **23**, 349–354.
42 G. S. Grest and K. Kremer, *Phys. Rev. A: At., Mol., Opt. Phys.*, 1986, **33**, 3628–3631.
43 K. Kremer and G. S. Grest, *J. Chem. Phys.*, 1990, **92**, 5057–5086.
44 L. Verlet, *Phys. Rev.*, 1967, **159**, 98–103.
45 W. C. Swope, H. C. Andersen, P. H. Berens and K. R. Wilson, *J. Chem. Phys.*, 1982, **76**, 637–649.
46 A. W. Lees and S. F. Edwards, *J. Phys. C*, 1972, **5**, 1921–1929.
47 J. Nickolls, I. Buck, M. Garland and K. Skadron, *Queue*, 2008, **6**, 40–53.
48 M. Liebetreu, M. Ripoll and C. N. Likos, *ACS Macro Lett.*, 2018, **7**, 447–452.
49 M. Liebetreu and C. N. Likos, *Commun. Mater.*, 2020, **1**, 4.
50 E. Westphal, S. Singh, C.-C. Huang, G. Gompper and R. Winkler, *Comput. Phys. Commun.*, 2014, **185**, 495–503.
51 M. P. Howard, A. Z. Panagiotopoulos and A. Nikoubashman, *Comput. Phys. Commun.*, 2018, **230**, 10–20.
52 W. Mattson and B. M. Rice, *Comput. Phys. Commun.*, 1999, **119**, 135–148.
53 J. S. Sims and N. Martys, *J. Res. Natl. Inst. Stand. Technol.*, 2004, **109**, 267–277.
54 J. L. White, *J. Appl. Polym. Sci.*, 1964, **8**, 2339–2357.
55 L. Tubiana, A. Rosa, F. Fragiacomo and C. Micheletti, *Macromolecules*, 2013, **46**, 3669–3678.
56 W. Humphrey, A. Dalke and K. Schulten, *J. Mol. Graphics*, 1996, **14**, 33–38.
57 K. M. Kam, L. Zeng, Q. Zhou, R. Tran and J. Yang, *J. Manuf. Syst.*, 2013, **32**, 154–166.
58 M. P. Allen and D. J. Tildesley, *Computer Simulation of Liquids*, Oxford University Press Inc., New York, 1987 (2009).
59 R. B. Bird, O. Hassager, R. C. Armstrong and C. F. Curtiss, *Dynamics of Polymeric Liquids*, John Wiley & Sons, New York, 2nd edn, 1987.
60 J. Rudnik and G. Gaspari, *J. Phys. A: Math. Gen.*, 1986, **19**, L191–L193.